

Early Career Materials Researcher Research Letter



Flexoelectricity-driven periodic buckling in multilayer graphene bonded to compliant substrate

Mrityunjay Kothari, Department of Mechanical Engineering, University of New Hampshire, Durham, NH, USA; Department of Civil and Environmental Engineering, Massachusetts Institute of Technology, Cambridge, MA, USA

Kyung-Suk Kim, School of Engineering, Brown University, Providence, RI, USA

Address all correspondence to Mrityunjay Kothari at Mrityunjay.kothari@unh.edu

(Received 12 May 2022; accepted 16 August 2022)

Abstract

Flexoelectricity in multilayer graphene (MLG) buckling can stimulate kink-shaped crinkle formation. In the process, the bifurcation becomes subcritical and the suspended-MLG's crinkle curvature is localized to a narrow band of $\sim 2nm$ width. We extend the study to flexoelectric layers bonded to a soft elastic substrate. Elastic substrates can guide the morphology of MLG and produce periodic patterns. We show that MLG's flexoelectricity together with substrate elasticity can produce periodic crinkles, which qualitatively explains the grade-dependent mosaic spreading in highly oriented pyrolytic graphite (HOPG). Experimental measurements of HOPG's surface-slope variations indeed confirm curvature localization at the crinkle valleys and ridges.

Introduction

Recent works have highlighted a new form of electromechanical coupling in 2D materials, known as quantum flexoelectricity, which couples polarization to the curvature of the layer. [1-4] The origin of this coupling, as the name suggests, lies in the distortion of electron cloud upon bending of the layer, which makes flexoelectricity a universal phenomenon that can occur in all dielectric materials. In particular, quantum flexoelectricity in graphene has attracted a lot of attention due to the already impressive range of properties of graphene that hold immense promise for high-end technologies.^[5,6]

Authors have previously investigated the effect of flexoelectric coupling on the buckling of free-standing multilayer graphene (MLG) through a combination of experiments, DFT, and continuum modeling. [2-4] While a single layer graphene (SLG) indeed shows the supercritical sinusoidal buckling with gently varying curvature, i.e., a wrinkle [Fig. 1(a)], [7] MLG can show a new subcritical crinkle mode, which localizes the surface curvature in a narrow region of width $\sim 2 nm$ and gives the appearance of triangular kink-like mode [Figs. 1(b₁) and (b₂)]. The flexoelectric polarization, localized near the ridges, serves to reduce the overall potential energy of the system by enhancing intralayer and interlayer attractive interactions.

The unique combination of localized curvature and localized polarization make graphene crinkles a powerful tool to manipulate charged and polarizable molecules by means of macroscopic strain control. In Kothari et al.[4] authors have demonstrated the potential of this technique in two proof-of-concept experiments. Firstly, the authors showed the self-assembly of buckyballs (C₆₀) molecules along crinkle valleys. Secondly, the authors also showed the self-assembly of DNA molecules along crinkle valleys in long straight segments. While these

experiments clearly showcase the potential of graphene crinkles for self-assembly applications, moving beyond proof-ofconcept experiments necessitates development of techniques that can create many crinkles in a pre-programmed fashion and provide an easy way to control them simultaneously.

We introduce a new methodology to address this challenge by extending our analysis to MLG bonded to a softer elastic substrate. The addition of the substrate brings in a new length scale into the system and gives rise to periodic buckling patterns when the assembly is laterally compressed. Without electromechanical coupling, the layer-on-substrate system with a stiffer layer is known to show wrinkles of a characteristic wavelength. [8-10] We will focus on studying how the supplement of flexoelectricity in the layer affects the stability of the system and the buckling mode. In particular, we will show the range of material parameters for which the crinkle bifurcation exists. In Kothari et al. [3] we introduced a wrinkle-crinkle phase diagram of MLGs [Fig. 1(c)] which revealed that the shorter the span of a free-standing MLG, the more it tends to crinkle than wrinkle. This result implies that an MLG wrinkle on a substrate with a wavelength shorter than the critical value would lead to crinkle bifurcation. These findings suggest that bonding MLG to soft elastic substrates can be an effective way to program the self-organization of large number of MLG crinkles.

The organization of the paper is as follows. In Sect. Methodology: theoretical formulation, we develop the theoretical formulation for the stability analysis. We discuss the results in Sect. A word on the length scales, followed by reporting experimental observations in Sect. Results and discussion. We conclude the work with a discussion of open challenges in Sect. Experimental observations.



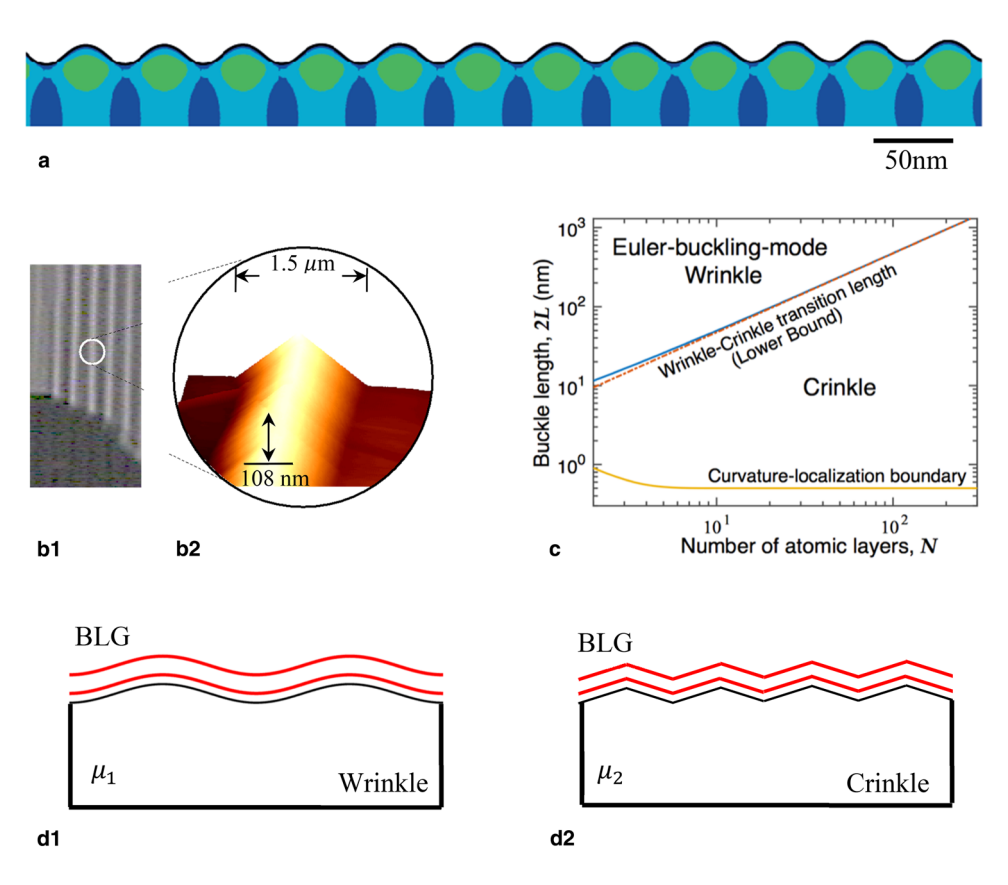


Figure 1. (a) Simulated SLG ($Q_b = 1.0 \text{eV}$) wrinkle on a PDMS substrate ($\mu = 0.3 MPa$) (b₁) MLG over PMMA groves (b₂) MLG crinkle. (c) Wrinkle-crinkle phase diagram of freely suspended MLG. Schematics of (d₁) BLG wrinkles and (d₂) BLG crinkles for $\mu_1 < \mu_2$.

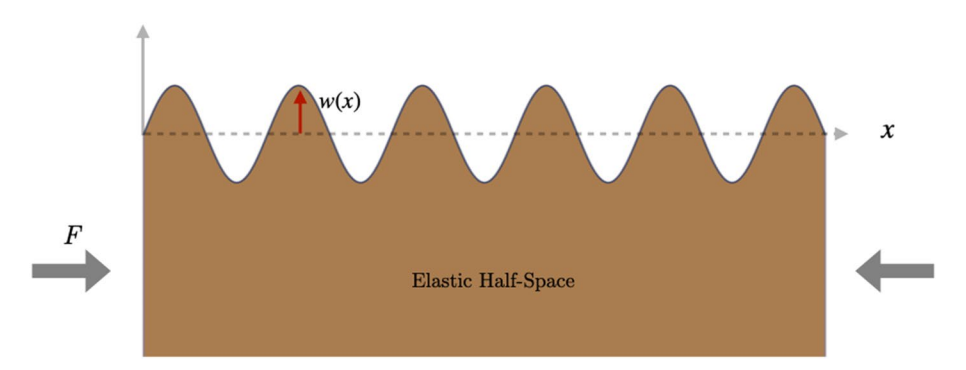


Figure 2. A schematic of the plane-strain setup.

Methodology: theoretical formulation

In this section, we will analyze the compressive buckling of a flexoelectric bilayer, e.g, a bilayer graphene (BLG), that is perfectly bonded to a soft elastic substrate, as depicted in [Fig. $1(d_1)$ and (d_2)]. The choice of bilayer is made for analytical convenience. The analysis can be extended to N-layers in an analogous way without any qualitative changes in the results. We will consider a plane-strain setting.

We introduce the following notation: Q_b is the bending stiffness per unit width of the individual layer, μ is the interlayer

shear stiffness, E and ν are the Young's modulus and Poisson's ratio of the substrate, respectively, a is the interlayer spacing, f is the lateral constraint force, w(x) denotes the vertical displacement of the free surface (Fig. 2), and T(x) denotes the normal traction at the interface between the bilayer and the substrate. We will assume the following kinematic assumptions: (a) layers are inextensible as $E_T/\mu \gg 1$, where E_T and μ are MLG's in-plane tensile and interlayer shear stiffness, respectively, and (b) both the layers of the bilayer deform in an identical fashion and maintain translational symmetry in

the thickness direction, as $E_N/\mu \gg 1$, where E_N is MLG's plane-normal tensile modulus.

We focus the analysis on classifying the buckling mode(s) and how they depend on the substrate stiffness. The equilibrium configurations of the system are those that minimize the total energy of the system, and can be obtained by the Euler-Lagrange equation for this system.

The total energy functional, Π , comprised mechanical and flexoelectric contribution from the flexoelectric bilayer, and mechanical contribution from the substrate. The energy contribution of the bilayer is

$$\Pi_{bilayer} = U_{mech} + U_{elec} \tag{1}$$

Here, the mechanical energy from bending and interlayer shearing is given as

$$U_{mech} = \int_{-L}^{L} \left(2 \frac{Q_b}{2} \left(\frac{d^2 w}{dx^2} \right)^2 + \frac{\mu a}{2} \left(\frac{dw}{dx} \right)^2 \right) dx.$$
 (2)

 U_{elec} is the electrostatic interaction energy in the bilayer (for a detailed discussion, refer to^[3]) and is given as

$$U_{elec} = \frac{-\beta_{(2)}^{*2}}{2\pi \epsilon_{(2)}} \int \int_{-L_0}^{L_0} \theta'(x)\theta'(\xi)g_{(2)}(\xi - x)dxd\xi, \quad (3)$$

where $\in_{(2)}$ and $\beta_{(2)}^*$ are the average permittivity and the effective flexoelectric constant of the bilayer, respectively. $g_{(2)}(x-\xi)$ is the dipole–dipole interaction kernel for bilayer and is given as ¹

$$g_{(2)}(\xi - x) = \frac{-(\xi - x)^2 + a^2}{\left\{ (\xi - x)^2 + a^2 \right\}^2} - \frac{2\{1 - q(\xi, x)\}}{(\xi - x)^2}$$
 (4)

$$q(\xi, x) = \begin{cases} 1/2, for |x - \xi| > r_0 \\ 1, for |x - \xi| \le r_0 \end{cases},$$

 $\theta(x) = w'(x)$ is the slope angle the layer makes with the x-axis, and r_0 is the cut-off radius of the interaction integration and is taken to be 0.15 nm for graphene.

Finally, the contribution of the substrate is given as

$$U_{sub} = \frac{1}{2} \int_{-L}^{L} T(x)w(x)dx. \tag{5}$$

The total potential energy Π is given by adding the energy contributions together with the inextensibility constraint,

$$\Pi = \int_{-L}^{L} \left(2 \frac{Q_b}{2} \left(\frac{d^2 w}{dx^2} \right)^2 + \frac{\mu a}{2} \left(\frac{dw}{dx} \right)^2 - f \left(\sqrt{1 + w'^2} - 1 \right) \right) dx + U_{elec} + U_{sub}.$$
 (6)

We employ here the bifurcation analysis technique that was first introduced in.^[3] By analyzing the Fourier Transform of the Euler-Lagrange equation for real and complex roots, we probe the bilayer for the existence of wrinkle or crinkle bifurcations.² If the roots are real, the bifurcation modes are sinusoidal, indicating wrinkle formation. If the roots are complex, some imaginary parts give exponentially decaying solutions of the curvature, implying curvature localization, i.e., crinkle formation.

Under the assumption of small displacements, the Euler-Lagrange equation is then obtained and its Fouriertransformed³ form becomes

$$2Q_b k^4 - k^2 (f - \mu a) - \frac{\beta_{(2)}^{*2}}{\pi \in (2)} k^4 \hat{g}_{(2)}(k) + \overline{E}k = 0, \quad (7)$$

where $\hat{T}(k) = \overline{E}k\hat{w}(k), \overline{E} = E/2(1-v^2)$.[11]

Fourier transform of the interaction kernel is given as

$$\hat{g}_{(2)}(k) = \pi |k| e^{-a|k|} + \pi |k| - 2kSi(kr_0) - \frac{2\cos(kr_0)}{r_0}$$
 (8)

The critical bifurcation wavenumber and the critical load can be found by recasting Eq. (7) as

$$f = \mu a + \left(2Q_b - \frac{\beta_{(2)}^{*2}}{\epsilon_{(2)}}\hat{g}_{(2)}(k)\right)k^2 + \frac{\overline{E}}{k}$$
 (9)

and subsequently minimizing f with respect to k. After we obtain f_{cr} , we plug it back into Eq. (7) and look for the solutions. Thus, the existence of complex roots of k_{cr} in physically meaningful range will indicate the existence of a crinkle bifurcation. As a consistency check, as the flexoelectricity vanishes,

the critical load is given as $f_0 = \mu a + 6Q_b \left(\frac{\overline{E}}{4Q_b}\right)^{\frac{2}{3}}$ and the corresponding wavenumber is given as $k_0 = \left(\frac{\overline{E}}{4Q_b}\right)^{1/3}$, which are in agreement with classical (i.e., without flexoelectricity) results on wrinkling.^[5,6] A more general critical wavenumber of an N-layer film with vanishing flexoelectricity on a neo-

Hookean substrate is derived from^[9] as
$$k_0 = \Lambda \left\{ \frac{(1+\Lambda^2)\mu_{NH}}{2N\widehat{Q}_b} \right\}^{\frac{1}{3}}$$
,

where μ_{NH} is the neo-Hookean shear modulus and Λ the prestretch of the substrate. Once again, for an N-layer film, our solution converges to k_0 in the absence of flexoelectricity.

¹ The function $q(\xi, x)$ is designed to exclude $|\xi - x| < r_0$ for singular intralayer interactions, with r_0 being the cut-off radius.

Fourier Transform of the Euler-Lagrange equation for small deflection w(x) leads to $A(k)\widehat{w}(k) = 0$, where k is the wavenumber, $\widehat{w}(k)$ is the Fourier transform of w(x), and A(k) is obtained to be (7). Then, the roots of A(k) = 0 for nontrivial $\widehat{w}(k)$ provide the bifurca-

Fourier transform is defined as $\hat{\phi}(k) = \int_{-\infty}^{\infty} e^{-ikx} \phi(x) dx$.



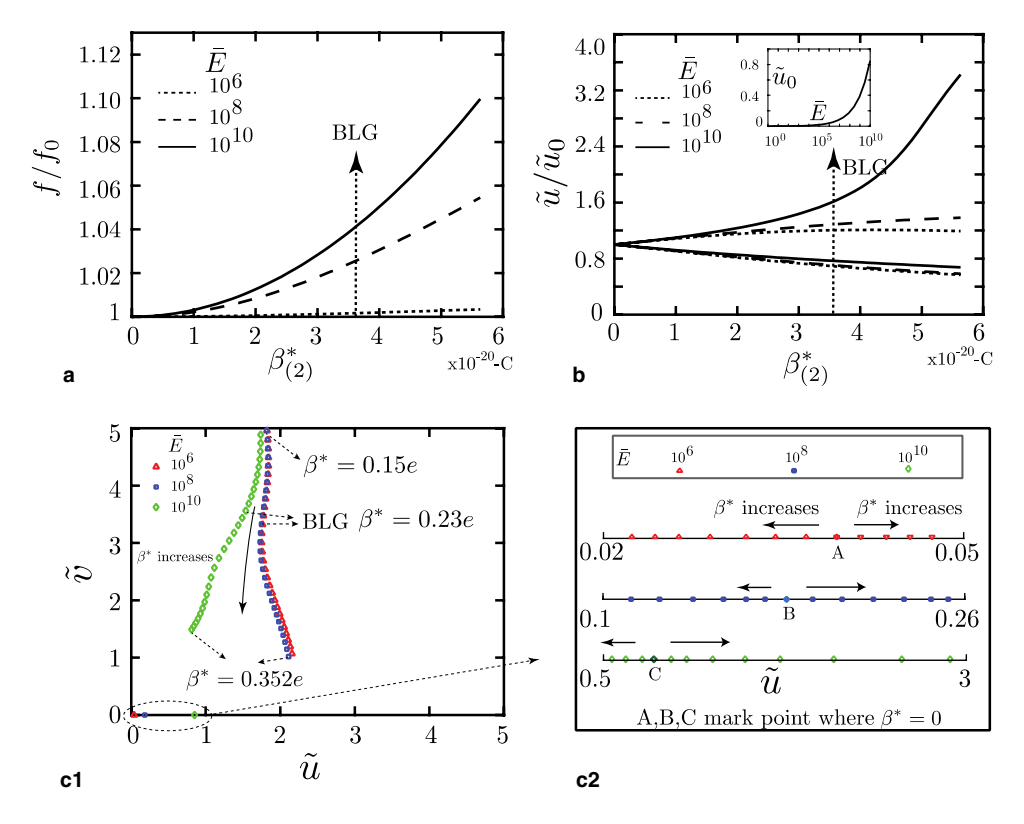


Figure 3. (a) Evolution of non-dimensional critical load. (b) Bifurcation of the real wavenumbers with the bifurcation parameter β^* . (c₁) Complex wavenumbers and (c₂) real wavenumbers given by the solution of (7) for different substrate stiffness. (c₁) shows the existence of crinkle bifurcation for BLG. Material parameters are chosen as reported in^[3]: $Q_b = 1.0 \text{eV}$, interlayer shear stiffness $\mu = 4GPa$, a = 0.34nm. \overline{E} units in Pa.

A word on the length scales

Prior to the analysis and interpretation of the results, it is instructive to examine the various length scales that appear in this problem. Interlayer spacing a is a material length scale for graphene. Since we employ a cut-off radius formulation for counting intralayer energy interactions, we introduce a length scale r_0 which is taken to be same as the lattice parameter for graphene. Consideration of the substrate adds a new length scale to the problem that typically decides the periodicity of the surface pattern as is well known from the study of layeron-substrate elastic systems.^[8] In analyzing the results from bifurcation analysis, it is important to note that the range of wavelength of interest is decided by two length scales—lower limit is the cut-off radius and the upper limit is the maximum wavelength predicted for layer-on-substrate system.^[8] Thus, for physically meaningful results, we restrict our range of interest to $\tilde{u} \in (0, 4.3), \tilde{v} \in (-5, 5)$, where k = u + iv and $\tilde{0}$ denotes nondimensionalization of wavenumber with a, which for graphene is taken to be 0.34 nm.

Results and discussion

In this section, we will focus on the onset of bifurcation and how the characteristic wavenumber changes with the inclusion of flexoelectricity and substrate. We start by looking at the variation of f_{cr} as the effective flexoelectric coefficient changes. Figure 3(a) shows that with increasing β^* , f_{cr} increases monotonically for different substrate stiffnesses. The indicator line marks β^* for graphene. We noticed that if the flexoelectric constant is increased beyond a certain limit, the f_{cr} becomes negative indicating that layer can spontaneously buckle and is unstable in its flat state, but that region is beyond the scope of our current treatment.

The incipient wavenumber for the purely mechanical case, $\sqrt{\pi} > 1/3$ ignoring any flexoelectric interactions, is given as $k_0 = \left(\frac{\overline{E}}{4Q_b}\right)$ as discussed in the previous section. As β^* is increased beyond zero, the real solutions of Eq. (7) show a bifurcation as shown in [Fig. 3(b)]. The plot shows non-dimensionalized real roots of Eq. (7) for different substrates. At zero flexoelectric coefficient, there is a repeated root that bifurcates into two branches as the flexoelectric coefficient increases. One branch shows a smaller wavenumber than the purely mechanical case and the other branch shows a larger wavenumber. In addition to that, we investigate Eq. (7) for complex roots to probe the existence of crinkle bifurcation. Note that the imaginary part of the complex root controls the local exponential decay of the curvature, whereas the real part controls the local periodicity. Figure $3(c_1)$ shows a very interesting picture of the bifurcation landscape. We recall here that our range of interest is $\widetilde{u} \in (0, 4.3), \widetilde{v} \in (-5, 5)$. As β^* increases beyond zero, Eq. (7) starts to show complex roots as

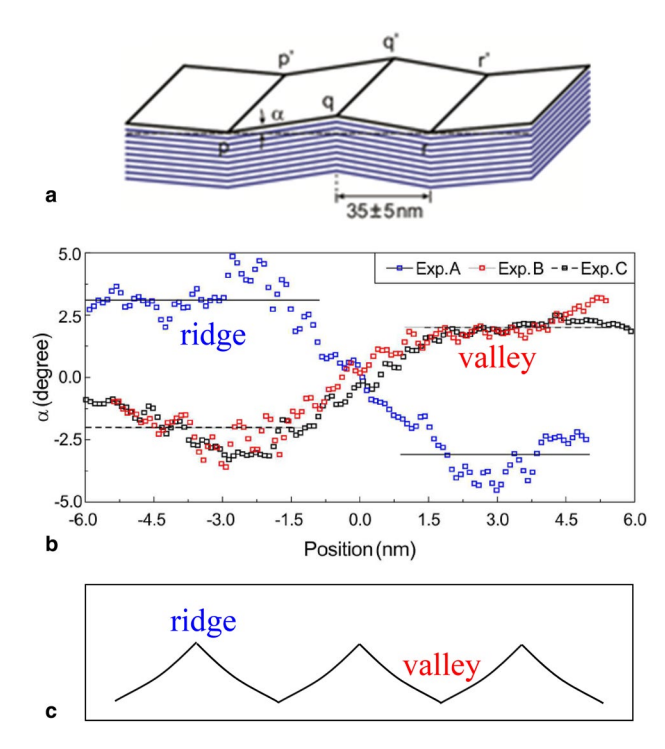


Figure 4. (a) A schematic of crinkles on a grade III HOPG. (b) Experimental measurement surface slopes across crinkle ridges and valleys. (c) A schematic of the grade III HOPG crinkles with different ridge and alley angles.

well in addition to two real roots. However, those roots are out of the physically admissible range. When β^* approaches a critical value that depends on \overline{E} , the complex roots begin to appear in our range of interest. This shows the clear existence of crinkle bifurcation for a flexoelectric bilayer attached to a softer substrate (arrows mark the bilayer graphene (BLG) case). For the range of \overline{E} shown in [Fig. 3(c₁)], the critical $\beta^* \sim 0.15e$. The flexoelectric coefficient for BLG is $\sim 0.23e$. As the flexoelectric coefficient increases beyond graphene's value, \tilde{u} remains nearly constant around ~ 1.8 for $\overline{E} < 10^8 Pa$, while \widetilde{v} decreases, thus making the oscillation persists over a longer width near the crinkle ridges or valleys. For higher \overline{E} ($\sim 10^{10} Pa$), we note that both \widetilde{u} and \widetilde{v} decrease indicating that wavelength of oscillations and the decay length become wider with increasing flexoelectricity. Figure $3(c_2)$ shows the evolution of real roots concurrently. The visible gap in [Fig. 3(c₁)] between $\overline{E} \le 10^8 Pa$ and $\overline{E} = 10^{10} Pa$ trends show that for higher \overline{E} , the competition between substrate elasticity and flexoelectricity determines the periodicity \tilde{u} , whereas for smaller \overline{E} , flexoelectricity dominates substrate elasticity, and therefore, \tilde{u} remains nearly unaffected by changes in \overline{E} .

We speculate that the post-buckling morphology will display a global periodicity dictated by the real roots [Fig. $3(c_2)$], and locally, the complex roots [Fig. $3(c_1)$] will serve to concentrate the curvature.

The bifurcation described in [Fig. $3(c_1)$] originates from the flexoelectricity of graphene layers. As the layers undergo

buckling, they develop curvature, which in turn creates flexoelectric dipoles normal to the bent layer (see also Fig. 4(b) in^[3]). These flexoelectric dipoles interact with each other—within the same layer as well as across layers; these interactions can be attractive (or repulsive), which will reduce (or increase) the total potential energy of the system (see also Fig. 3(f) in^[3]). The unique complex bifurcation observed in crinkles, which localizes the surface curvature to a narrow width (controlled by the imaginary part of the wavenumber) together with the curvature reversal (controlled by the real part of the wavenumber), enables them to reduce the potential energy of the system significantly as compared to a wrinkle mode bifurcation, which does not localize surface curvature and shows only real solutions.

As described by the authors previously, [3] a flexoelectric crinkle parameter governs the existence of crinkles. We expect the parameter to have a similar effect even in the layer-onsubstrate case. Figure 3 shows that for smaller flexoelectric constants, the complex solutions are outside of the range of interest. Speaking in physical terms, the flexoelectric interactions are not strong enough to cause crinkles to form, and the mechanical modality dominates. As the flexoelectricity effect becomes stronger, the system starts to show crinkle bifurcation.

Experimental observations

The MLG crinkle configurations could be observed with AFM imaging for relatively thick suspended MLGs as seen in Fig. 2(a-2) and (b-2) in [2]. A schematic of a MLG crinkle ridge is shown in [Fig. 4(a)]. However, the bluntness of the AFM tip and the attraction force of the MLG's flexoelectric surface charge prevent accurate tracing of the surface profile near the curvature-localized valleys and ridges of the crinkle. TEM or SEM imaging would be distorted by the crinkle charges as well. So far, the most accurate measurement of the crinkle surface profile near the MLG crinkle's curvature localization could be made with an AFM atomic lattice interferometry (ALI).^[14] Here, we present the AFM-ALI measurement of the surfaceslope variations across the valleys and ridges of HOPG crinkles, i.e., boundaries of mosaic patterns, in Fig. 4(b).

Regarding MLG films on an elastic substrate, a wide variety of graphene corrugation morphologies on different substrates were reviewed in [12]. The most noticeable crinkle morphology observed in nature is the mosaic patterns on an HOPG surface. A schematic of a crinkle ridge on a grade ZYH HOPG with the mosaic spread^[13] of $\sim 3.5^{\circ} \pm 1.5^{\circ}$ is illustrated in Fig. 4(a). The wavelength of the crinkle mosaic pattern is measured ~ 70 nm in our AFM measurements (not shown here). The AFM-ALI measurements show that the surface-slope angle varies approximately from $+3.0^{\circ}$ to -3.0° across a ridge of a ~ 3 nm localizedcurvature crinkle. In contrast, the slope changes approximately from -2.2° to $+2.2^{\circ}$ across a crinkle valley. These variations are within the mosaic spread bounds measured by the crystallographic X-ray peak spreading of the Cu-Kα rocking curve [13]. Figure 4(c) illustrates a schematic of the HOPG surface crinkle pattern. Higher grades, ZYA and ZYB, of HOPG have much



smaller mosaic spread angles, $\sim 0.4^{\circ} \pm 0.1^{\circ}$ and $\sim 0.8^{\circ} \pm 0.2^{\circ}$, respectively, with longer crinkle wavelengths than those of ZYH.

Considering the mean defect-free depth (MDFD) of the HOPG near its surface as an effective thickness of an MLG film on an elastic substrate, the MDFD of the HOPG is thicker, i.e., the effective N is larger, and the corresponding wavelength is longer for higher grades. The grade-dependent crinkle wavelength and the surface slope angle variations are qualitatively consistent with the analytical prediction of the wavelength and the decay length dependence on the effective number of layers, N. However, it is left for future work to quantitatively model MLG buckling on an anisotropic elastic substrate and evaluate the effective compressive film stresses developed during the high-temperature manufacturing process of HOPG.

Conclusion and outlook

We carried out the bifurcation onset analysis and predicted the critical wavelength for layer-on-soft-substrate system in this chapter. To comment on the nature of the bifurcation, it is important to analyze the post-buckling evolution as well. Free standing crinkles show a subcritical bifurcation, and we expect the substrate stiffness to possibly alter it for certain range of stiffness. A finite element modeling of this system would help characterize the post-buckling evolution accurately and can handle large deformations as well as extensibility and interlayer normal compliance. To the best of our knowledge, such a study has not been previously conducted. This work can also be extended to other 2D materials beyond graphene by carrying out atomistic studies to characterize flexoelectricity and subsequently analyzing the bifurcation landscape using the machinery developed in this work.

Addition of the substrate into the framework adds another length scale that depends on \overline{E} . The authors have previously developed a quantum flexoelectric crinkle parameter that arises out of combination of bending and flexoelectricity-induced stiffness. Another non-dimensional parameter^[3] comprising flexoelectricity and substrate properties can be formulated and subsequently used to study the crinkle-wrinkle transition in the layer-on-substrate case. Lastly, we note that soft substrates typically demonstrate dielectricity, and therefore, a more refined formulation must consider the dielectric interactions between the layer and the substrate. Nevertheless, the results of the simplified model are consistent with experimental measurements of HOPG's surface slope variations and qualitatively elucidate the grade-dependent mosaic spreading in HOPG which could not be explained previously.

Acknowledgments

Support from the U.S. National Science Foundation and assistance of C.-K. Wang in operating a Park Systems AFM to get Fig. 4(b) are gratefully acknowledged.

Funding

U.S. National Science Foundation Award Number: 193414.

Data availability

All data generated or analyzed during this study are included in this published article.

Declarations

Conflict of interest

The authors declare no conflict of interest.

References

- S.V. Kalinin, V. Meunier, Electronic flexoelectricity in low-dimensional systems. Phys. Rev. B 77(3), 033403 (2008)
- R. Li, M. Kothari, A.K. Landauer, M.-H. Cha, H. Kwon, K.-S. Kim, A new subcritical nanostructure of graphene—crinkle-ruga structure and its novel properties. MRS Advances 3, 1–7 (2018)
- M. Kothari, M.-H. Cha, K.-S. Kim, Critical curvature localization in graphene. i. quantum-flexoelectricity effect. Proc. R. Soc. A 474(2214), 20180054 (2018)
- M. Kothari, M.-H. Cha, V. Lefevre, K.-S. Kim, Critical curvature localization in graphene. ii. non-local flexoelectricity-dielectricity coupling. Proc. R. Soc. A 475(2221), 20180671 (2019)
- C.E. Machnicki, F. Fu, L. Jing, P.Y. Chen, I.Y. Wong, Mechanochemical engineering of 2D materials for multiscale biointerfaces. J. Mater. Chem. B 7(41), 6293–6309 (2019)
- S. Krichen, P. Sharma, Flexoelectricity: A perspective on an unusual electromechanical coupling. J. Appl Mechanics 10(1115/1), 4032378 (2016)
- J.H. Jung, J.K. Bae, M.-W. Moon, K.-S. Kim, J. Ihm, Numerical study on sequential period-doubling bifurcations of graphene wrinkles on a soft substrate. Solid State Commun. 222, 14–17 (2015)
- 8. Allen, H., (1969) Analysis and structural design of sandwich panels
- 9. T.W. Shield, K.-S. Kim, R.T. Shield, The buckling of an elastic layer bonded to an elastic substrate. J. Appl. Mech. 61, 231–235 (1994)
- J.-Y. Sun, S. Xia, M.-W. Moon, K.H. Oh, K.-S. Kim, Folding wrinkles of a thin film stiff layer on a soft substrate. Proc. R. Soc. A 468(2140), 932–953 (2012)
- Z.Y. Huang, W. Hong, Z. Suo, Nonlinear analyses of wrinkles in a film bonded to a compliant substrate. J. Mech. Phys. Solids 53(9), 2101–2118 (2005)
- S. Deng, V. Berry, Wrinkled, rippled and crumpled graphene: an overview of formation mechanism, electronic properties, and applications. Mater. Today 19(4), 197–212 (2016)
- M. Ohler, J. Baruchel, A.W. Moore, P. Galez, A. Freund, "Direct observation of mosaic blocks in highly oriented pyrolytic graphite." Nucl. Instrum. Methods Phys. Res Sect. B 129, 257–260 (1997)
- B.K. Jang, J. Kim, H.J. Lee, K.-S. Kim, C.K. Wang, Device and method for measuring distribution of atomic resolution deformation United States Patent. Patent Number 9(003), 561 (2015)